IEEE Photonics Journal
An IEEE Photonics Society Publication

Toward High-Power Terahertz Emitters Using Large Aperture ZnSe Photoconductive Antennas

Volume 3, Number 2, April 2011

X. Ropagnol
R. Morandotti
T. Ozaki
M. Reid

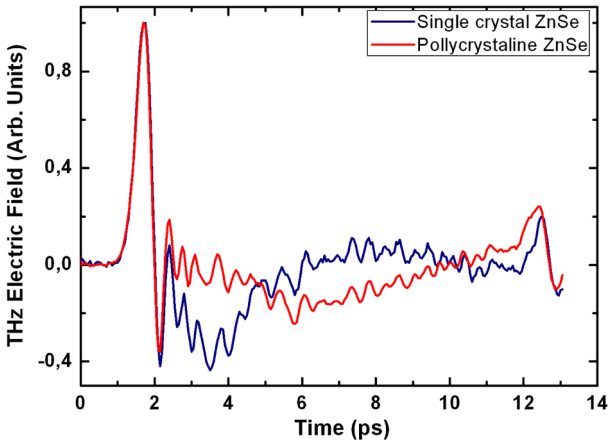

DOI: 10.1109/JPHOT.2011.2116112
1943-0655/$26.00 ©2011 IEEE

IEEE photonics SOCIETY
IEEE

Toward High-Power Terahertz Emitters Using Large Aperture ZnSe Photoconductive Antennas

X. Ropagnol,[1] R. Morandotti,[1] T. Ozaki,[1] and M. Reid[2]

[1]INRS-EMT, Advanced Laser Light Source, Université du Québec, Varennes, QC J3X 1S2, Canada
[2]Department of Physics, University of Northern British Columbia, Prince George, BC V2N 4Z9, Canada

DOI: 10.1109/JPHOT.2011.2116112

Manuscript received December 8, 2010; revised February 10, 2011; accepted February 10, 2011. Date of publication February 15, 2011; date of current version March 4, 2011. Corresponding author: X. Ropagnol (e-mail: ropagnol@emt.inrs.ca).

Abstract: We investigate the generation of free-space terahertz (THz) radiation from photoconductive antennas using single crystal and polycrystalline ZnSe substrates. The photoconductive antennas have been excited above (400 nm) and below (800 nm) the bandgap. We investigate the dependence of the THz electric field radiated from biased ZnSe emitters on the applied bias field and on the incident optical fluence for bias fields as high as 26 kV/cm and for optical fluences of 0.005–3 mJ cm^{-2}. The saturation fluence is observed to be significantly different both above and below bandgap excitation. These results show that, in comparison with GaAs substrates, ZnSe has strong potential as a high-power THz emitter.

Index Terms: Terahertz (THz) sources, semiconductor materials, second harmonic generation, terahertz, two-photon processes.

1. Introduction

The generation of radiation at terahertz (THz) frequencies has become a well-established technique, with many applications in both science and technology [1]. There has been a recent surge in the research conducted on generating high-energy, ultrashort THz pulses, which is being driven by applications in imaging [2], [3], security [3], [4], and THz spectroscopy [3], [5]. Recently, single-cycle THz pulses with 1.5 μJ energy and an energy conversion efficiency of 3.1×10^{-5} have been generated via optical rectification in a large-aperture ZnTe crystal [6]. Another method to generate high-energy THz pulses is by phase matching between an optical pulse and a THz pulse using the tilted-pulse-front technique to overcome the large difference in the refractive index at 800 nm and at submillimeter wavelengths [7]–[10]. Stepanov *et al.* have generated 30 μJ, single-cycle THz pulses using 28-mJ femtosecond optical pulses, giving an optical-to-THz conversion efficiency of 1.1×10^{-3} [11] using a long $LiNbO_3$ crystal. The tilted-pulse-front technique induces strong dispersion of the 800-nm pulse during the propagation inside the long crystal [12], which leads to a relatively narrow THz spectrum and a longer pulse width. Such novel, intense THz sources are currently allowing researchers to conduct new experiments and to study the nonlinear optical response of materials at THz frequencies and at picoseconds timescales. Techniques such as optical-pump/THz-probe, THz-pump/THz-probe, and open aperture Z-scan experiments have been used to explore the nonlinear electron dynamics of semiconductor crystals such as GaAs and InGaAs [13]–[15]. Moreover, strong saturation of free carrier absorption in n-doped GaAs and InSb at THz frequencies has been demonstrated by using THz-pump/THz-probe techniques [16]. Recently, intense THz

sources have enabled the study of the Kerr effect, in which a THz intensity-dependent birefringence is induced in liquids at THz frequencies [17].

Since intense THz sources based on optical rectification involve the conversion of infrared photons to THz photons, the maximum efficiency of THz generation via optical rectification is limited to approximately 10^{-3}. In contrast, the large aperture photoconductive antenna (LAPCA) is an attractive method to overcome such limitations, since THz radiation from these sources is extracted from an externally applied bias field [18]. To date, the largest optical-to-THz conversion efficiency was obtained with a LAPCA, and was 1.6×10^{-3} [19]. Half-cycle THz pulses have been generated with 0.8-μJ energy from a 3.5-cm gap GaAs antenna and a pulsed bias voltage of 48 kV.

The mechanism of THz generation from biased photoconductive antennas can be understood using the current-surge model [18]. A femtosecond, pulsed laser illuminates the gap of a semiconductor crystal and creates carriers in the conduction band. An external bias field accelerates the carriers up to the saturation velocity, leading to a transient photocurrent. This transient current radiates an electromagnetic field at the surface of the semiconductor. From Maxwell's equations, the THz electric field in the far field is proportional to the time derivative of the transient current [18], which can be expressed as [20]

$$E(t) \propto \frac{\partial J}{\partial t} \propto E_b \frac{dn(t)}{dt}. \tag{1}$$

Here, J is the current density, E_b is the applied bias field, and n is the carrier density. From (1), we can see that the THz electric field scales linearly with the applied bias electric field.

An important saturation process for the large aperture photoconductive antenna is the screening of the bias field by the emitted THz field [18], [21], [22]. This saturation process limits the THz energy conversion efficiency. The conversion efficiency depends on the optical excitation fluence F and can be written as [23]

$$\eta = \frac{\tau E_b^2}{2F\eta_0} \left(\frac{F}{F + F_{\text{sat}}} \right)^2. \tag{2}$$

Here, τ is the time duration of the THz pulse, η is the impedance of free space, and F_{sat} is the saturation fluence of the photoconductor. We can write F_{sat} as [22]

$$F_{\text{sat}} = \frac{h\nu(1 + \sqrt{\varepsilon})}{e\mu\eta_0(1 - R)}. \tag{3}$$

Here, $h\nu$ is the photon energy of the pump laser and e is the electron charge. Equation (3) shows that the saturation fluence depends on various parameters of the photoconductive substrate, such as the dielectric constant, carrier mobility μ, and the reflectivity R of the substrate at the laser wavelength.

We also define the maximum conversion efficiency η_{max}, which is obtained when we generate THz radiation with an excitation fluence equal to the saturation fluence [23]

$$\eta_{\text{max}} = \frac{\tau E_b^2}{8F_{\text{sat}}\eta_0}. \tag{4}$$

As we can see in (4), the maximum conversion efficiency is proportional to the square of the bias field and inversely proportional to the saturation fluence, which in turn is inversely proportional to the mobility. Consequently, the maximum conversion efficiency is linearly proportional to the mobility. Many works on THz generation from photoconductive antennas have used GaAs and InP crystals as substrates, since they can be pumped above the bandgap with Ti:sapphire lasers. Both crystals have large carrier mobilities and high breakdown voltages (for example, 3000 cm^2/Vs and 10 kV/cm, respectively, for GaAs).

Equation (1) shows that the maximum THz electric field is determined by the bias field. For this reason, wide bandgap semiconductor crystals are very attractive. Unfortunately, wide bandgap

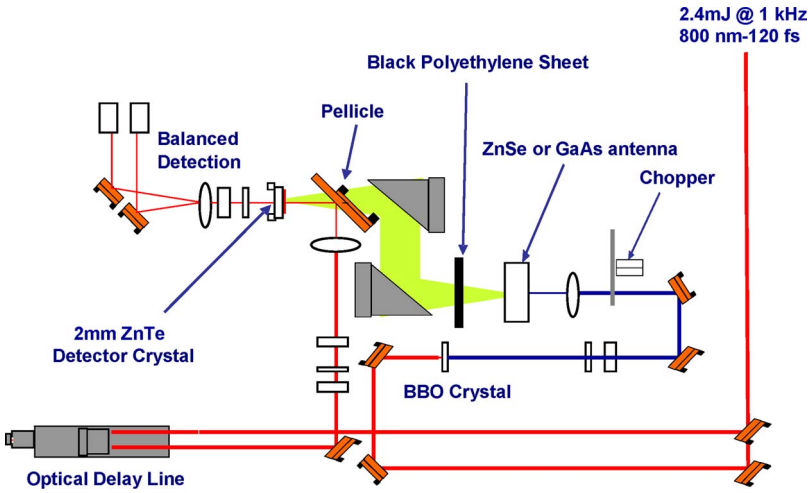

Fig. 1. Experimental setup for the generation and the detection of THz radiation from biased photoconductive antennas.

semiconductor crystals (with a large dielectric strength) also have lower mobility, which tends to decrease the THz energy conversion efficiency. Diamond is a natural alternative as a substrate to improve the magnitude of the radiated THz electric field, and the THz energy conversion efficiency, because of its very high breakdown voltage (1000 kV/cm), despite its very low mobility (10 cm^2/Vs) [24]. However, efficient operation of diamond switches requires pumping above its high bandgap (5.6 eV), which in turn requires high-energy ultraviolet laser pulses that are difficult to generate and work with.

A good compromise between GaAs and diamond is ZnSe. ZnSe has high dielectric breakdown strength (over 70 kV/cm [25]) and a carrier mobility of approximately 140 cm^2/Vs [26]. ZnSe also has a bandgap of 2.67 eV, and therefore, above-bandgap pumping is possible with the second harmonic of a standard Ti:sapphire laser or by pumping below the bandgap at 800 nm via a two-photon absorption process. CVD polycrystalline ZnSe antennas have previously been studied [27]. For example, micrometer-scale antennas have been pumped below the bandgap (800 nm), and it was demonstrated that CVD polycrystalline ZnSe could be pumped up to 28 mJ cm^{-2} without observing any saturation of the radiated THz electric field, and a bias field as high as 120 kV/cm could be applied without breakdown of the crystal.

In this report, we perform systematic investigations of THz radiation emitted from ZnSe photoconductive antennas. The work presented here examines both mono- and polycrystalline ZnSe excited both above and below the bandgap, as well as the scaling of THz emission with the applied bias field and the optical excitation fluence. The motivation for this work is to determine the suitability of ZnSe LAPCAs for generating high THz pulse energies, which is timely given the recent interest in such sources. We also compare THz radiation from single crystal ZnSe and polycrystalline ZnSe with GaAs antennas to explicitly demonstrate that single crystal ZnSe antennas holds strong potential as a high-power THz emitter.

This paper is presented as follow. In Section 2, the experimental setup is presented. In Section 3, we present our experimental results with ZnSe antennas. Then, in Section 4, we discuss the optical-to-THz energy conversion efficiency of ZnSe antennas. We also discuss the advantages and the consequences of working with ZnSe photoconductive antennas instead of GaAs antennas.

2. Experimental Setup

Fig. 1 shows the experimental setup used to generate and detect THz radiation from externally biased photoconductive antennas. We used an amplified Ti:sapphire laser with a 2.4-mJ pulse energy, 800-nm center wavelength, and a 120-fs pulse duration, operating at 1 kHz repetition rate.

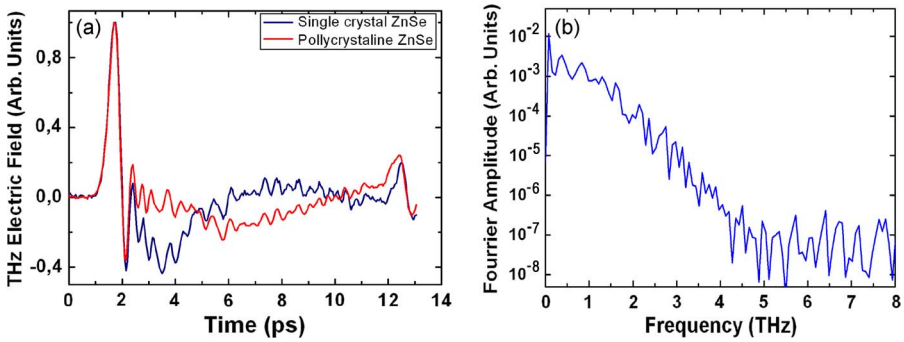

Fig. 2. Typical normalized THz pulse waveform of ZnSe single crystal and polycrystalline ZnSe antenna (a) and Fourier amplitude of the waveforms of the THz pulse from polycrystalline ZnSe antenna (b).

The Ti:sapphire laser beam is split into two paths using a beam splitter. Ninety percent of the laser energy is used in the pump path, and the remaining 10% is used in the probe path. A beta Barium Borate (beta BaB_2O_4) crystal in the pump path is used to generate the second harmonic of the Ti: sapphire laser, which in turn is used to pump the ZnSe antenna above the bandgap. The BBO crystal is removed when we pump the antenna at 800 nm. GaAs, mono-, and polycrystalline ZnSe antennas were investigated. Electrical contacts were formed with silver paint. Electrodes are placed on opposite sides of the crystal surface to avoid breakdown in air. All substrates used in this study were 0.5 mm thick and polished on both sides. The electrode width is 2 mm, and the gap size is 1 mm. Silicon epoxy covers the silver paint electrodes to avoid corona discharge [28]. The external bias field is provided by a DC power supply. THz radiation is radiated into free space and is collected by a pair of f/2 off-axis parabolic mirrors. Two layers of black polyethylene placed after the antenna blocked any 800- or 400-nm pump leakage. The ZnSe antenna was illuminated above the bandgap using a lens, which reduces the beam size and consequently increases the fluence. The antenna was placed before the focus, where the beam diameter was measured to be 3 mm using a knife-edge technique. The emitted THz wave was detected by time-resolved electrooptic sampling with a 1-mm-thick [110] ZnTe crystal [29]. The ZnTe crystal was oriented so that the (001) direction was parallel to the polarization of the THz field. The probe was focused using a 4-in focal length lens, and a pellicle beam splitter was used to reflect the probe beam so that it was collinear with the THz beam in the ZnTe detector crystal. Two balanced photodiodes detected the orthogonal polarization components of the probe split by a Wollaston prism. The THz waveform was recorded using a lock-in amplifier.

3. Experimental Results

3.1. THz Pulse Shape and Spectrum From ZnSe Antennas

Fig. 2 shows typical THz waveforms obtained using a mono- and polycrystalline ZnSe large aperture photoconductive antenna, with a gap size of 3 mm and 8 mm and a pump fluence of 250 μJ cm^{-2} and 350 μJ cm^{-2}. The bias field was 3.3 kV/cm and 3.1 kV/cm for mono- and polycrystalline ZnSe antenna, respectively.

In this experiment, one off axis mirror was used to focus the THz beam on the ZnTe crystal detector. The waveforms were normalized to unity in order to compare the shape of the two waveforms. In Fig. 2(a), we observe an initial positive pulse with a full-width at 1/e-maximum temporal duration of 560 fs, followed by a very long negative tail, which is similar for both waveforms. A shorter negative tail (3 ps) appears for the ZnSe single crystal (compared with a 6-ps tail for polycrystalline ZnTe), which can be understood based on the faster decay of the transient photocurrent in single crystals. X-ray diffraction (XRD) measurements indicate that the ZnSe single crystal wafers contained iron impurities. The faster decay can therefore be explained by the presence of more defects in the ZnSe single crystal due to a slight doping of iron, which leads to a faster carrier recombination rate. The oscillations in the waveforms result from water absorption,

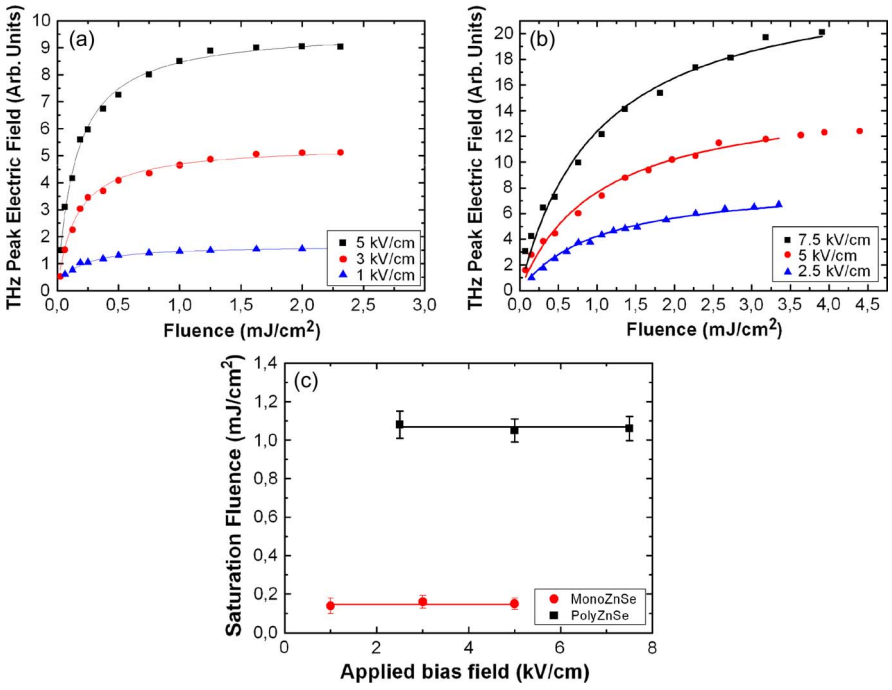

Fig. 3. Fluence dependence of the peak THz electric field at several values of bias fields for (a) ZnSe single crystal antenna and (b) polycrystalline ZnSe antenna. Solid lines indicate best fitted curves with a saturation fluence of 0.15 mJ cm^{-2} for single ZnSe crystal and 1.01 mJ cm^{-2} for polycrystalline ZnSe and (c) the saturation fluence dependence versus bias fields for mono- and poly-crystalline ZnSe antennas.

and the small positive peak at 12 ps is a reflection from the ZnSe crystal. Fig. 2(b) shows the spectral intensity of the THz spectrum for a polycrystalline ZnSe antenna, which extends to above 4 THz. Dips in the spectrum at 1.4, 1.85, 2.22, and 2.4 THz are due to the strong water absorption lines in the THz frequency range [30]. The additional modulation in the frequency spectrum can be attributed to multiple reflections of the THz pulse in the ZnSe crystal emitter. The spectrum is comparable with that obtained experimentally using a GaAs large aperture photoconductive antenna [31], [32].

3.2. Scaling of the Radiated THz Field With Optical Excitation Fluence

In what follows, it is important to note that the values reported for the peak THz electric field are in arbitrary units. Calibration of the peak THz electric field was difficult, due to insufficient THz pulse energies for detection by an infrared camera or a pyroelectric detector. However, the values of the peak field plotted on the same graph have the correct relative magnitudes, but those magnitudes are not simply related between different graphs. The reason for this is that probe power, lock-in amplifier constants, and other parameters that affect the magnitude of the detected signal were varied in the different experiments.

In Fig. 3(a) and (b), the peak electric field radiated from mono- and polycrystalline ZnSe photoconductive antennas is plotted as a function of the optical excitation fluence for three different bias voltages. The antennas were illuminated with pump photon energies above the bandgap (400 nm). As expected, the THz peak electric field is proportional to the bias electric field and the pump fluence. All data in the figure have been fitted using (5), which takes into account the saturation behavior of the THz field amplitude [6]–[17]

$$E_{\mathrm{rad,THz}} \approx \beta\left(\frac{F}{F + F_{\mathrm{sat}}}\right). \tag{5}$$

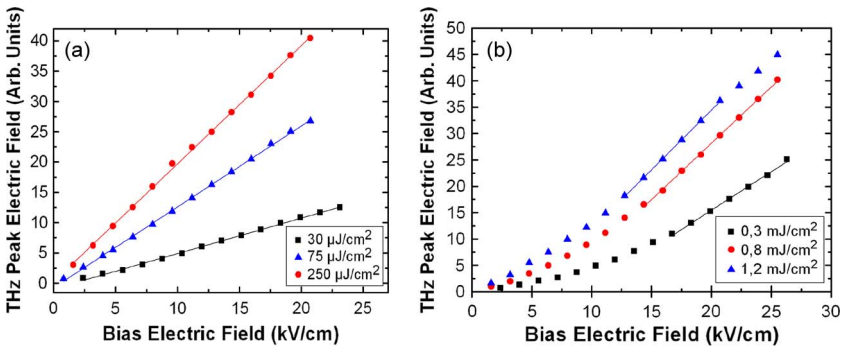

Fig. 4. Bias field dependence of peak THz field from a ZnSe single crystal photoconductive antenna (a) and from a polycrystalline ZnSe antenna (b) illuminated above the bandgap for three different fluences.

Here, β is a constant reflecting the amplitude of the radiated field, which depends on the applied bias field.

In Fig. 3(a) and (b), the points are the experimentally measured values, and the solid curves are fits to the data using (5). The peak THz field plotted as a function of the fluence shows clear saturation behavior. By fitting the experimental data with (5), the saturation fluence was measured to be 0.15 ± 0.02 mJ cm^{-2} and 1.09 ± 0.07 mJ cm^{-2} for mono- and polycrystalline ZnSe antennas, respectively. Using these values in (3), we obtained a carrier mobility of 267 cm^2/Vs for single crystal ZnSe and 40 cm^2/Vs for polycrystalline ZnSe. The carrier mobility for ZnSe single crystal is higher than expected, which is due to iron impurities, which increases the carrier mobility.

In Fig. 3(c), the saturation fluence is plotted as a function of the applied bias field. The saturation fluence is found to be independent of the applied bias field, which is particularly important for scaling the THz antennas to higher output pulse energy. This is because the conversion efficiency is a strong function of the bias field and saturation fluence, and thus, for (4) to be a reasonable approximation, the saturation fluence must be independent of the bias field. The results presented in Fig. 3(c) shows that this is indeed the case for both mono- and polycrystalline ZnSe.

3.3. Scaling of the Radiated THz Field With Applied Bias Field

In this section, we study the dependence of the bias field on the THz emission from mono- and polycrystalline ZnSe antennas excited above the bandgap. In Fig. 4, we present the peak field of the THz pulse from (a) ZnSe single crystal antenna and from (b) polycrystalline ZnSe antenna as a function of the bias electric field for three different fluences. The three fluences are 3×10^{-2}, 7.5×10^{-2}, and 0.25 mJ cm^{-2} for the ZnSe single crystal antenna and 0.3, 0.8, and 1.2 mJ cm^{-2} for the polycrystalline ZnSe antenna. These three different fluences have been chosen so that one is lower than the saturation fluence, the second is approximately equal to the saturation fluence, and the third is higher than the saturation fluence of both crystals.

From Fig. 4(a), a linear dependence of the THz electric field is observed with the bias field up to 23 kV/cm for ZnSe single crystal for the three different fluences. At higher applied bias fields, strong corona discharge was observed that damaged the crystals and reduced the emitted THz radiation. From Fig. 4(b), we do not see a linear dependence of the peak THz field for polycrystalline ZnSe antenna. This behavior has previously been reported in GaAs antennas [20]. The nonlinear behavior was attributed to the nonohmic resistance in the metal contact of the semiconductor. In our case, we observe a quadratic dependence at low bias field that becomes linear for bias fields higher than 15 kV/cm. Also, consistent with what was reported in [20], the field threshold decreases with increasing laser fluence as the conductivity of semiconductors crystal increases with increasing carrier density. For the highest fluence, we observe the onset of saturation of the peak THz electric field starting at 23 kV/cm. This may come from heating in the crystal with these higher

bias voltages, which induce corona discharges reducing the bias voltage and limiting the THz emission.

3.4. THz Emission Characteristics of ZnSe Antennas Excited Above and Below the Bandgap

In Fig. 5, the peak THz electric field from a ZnSe single crystal photoconductive antenna is plotted as a function of the excitation fluence, when pumped above ($\lambda = 400$ nm) and below ($\lambda = 800$ nm) the bandgap ($E_g = 2.67$ eV). The applied bias voltage was 3 kV/cm. A strong saturation of the peak THz electric field is observed in both cases, saturating to the same value. The saturation of the peak THz field begins at a lower fluence when pumped at $\lambda = 400$ nm compared with excitation below the bandgap. This is expected since the latter is driven via two-photon absorption, in comparison with direct linear absorption in the former process. The peak THz electric field, when excited at 400 nm, follows (7). At 800 nm, the behavior of the peak THz electric field is completely different. Because of the nonlinear absorption process, the THz peak electric field increases quadratically at low fluence. For high fluence, we observe a linear dependence of the THz peak electric field from 0.7 mJ cm^{-2} up to 2.1 mJ cm^{-2}. At even higher fluence, the THz peak electric field saturates to a value similar to that observed at 400 nm. If we define the saturation fluence to be when the THz emission is one half of the maximum peak THz field that is radiated, we obtain a saturation fluence of 1.23 mJ cm^{-2} for below the bandgap excitation. In comparison, the saturation fluence of the ZnSe single crystal antenna excited above the bandgap is only 150 μJ cm^{-2}. In order to achieve the highest optical-to-THz energy conversion efficiency, it is therefore necessary to drive ZnSe antennas above the bandgap. We have also observed that when the antenna is pumped at 800 nm, the antenna lifetime is reduced as a result of corona discharges that are created at the surface of the crystal.

3.5. Comparison of THz Emission From ZnSe and GaAs Antennas

In this section, we compare the performance of GaAs and ZnSe antennas. This comparison is useful for two reasons: i) to estimate the optical-to-THz energy conversion efficiency and to compare it with the most common LAPCA and ii) to evaluate the scalability of THz emission from ZnSe single crystal antennas to determine if it has the potential to be a useful high-energy THz source.

In Fig. 6, the peak THz electric field from GaAs, ZnSe single crystal and polycrystalline ZnSe photoconductive antennas is plotted as a function of the excitation fluence. The bias voltage is fixed at 2.5 kV/cm for the three different antennas. The GaAs antenna was excited at 800 nm and the mono- and polycrystalline ZnSe antennas at 400 nm. The points are the experimental data and the solid lines are the best-fit curves to the data using (5).

All antennas have the same design with a gap size of 1 mm and an electrode width of 2 mm. From Fig. 5, we can see that the THz emission from the GaAs antenna is saturated at low excitation fluence, which is in agreement with observations by many groups [16], [19], [27]. We can also observe a clear saturation of the THz peak electric field for the ZnSe single crystal antenna. Such a strong saturation of the THz electric field was not observed for the polycrystalline ZnSe antenna, even when illuminated with a fluence as high as 3.5 mJ cm^{-2}. It is expected that if the fluence could be increased even further, the THz peak electric field would saturate to the same value as for the GaAs and ZnSe single crystal antennas. It was not possible to increase the fluence further because the output second harmonic generation energy from the BBO crystal was a maximum for our laser system.

The difference between the three antennas can be explained by the difference in the carrier mobilities of the three crystals, resulting in three different saturations fluences. Fitting the data gives saturation fluences of $0.011 \pm 7 \times 10^{-4}$ mJ cm^{-2}, 0.15 ± 0.022 mJ cm^{-2}, and 1.07 ± 0.065 mJ cm^{-2} for the GaAs, mono- and polycrystalline ZnSe antennas, respectively. The second fitting parameter is the maximum THz peak electric field, whose values are 8.55 $\pm$ 0.11, 8.50 $\pm$ 0.13, and 8.52 $\pm$ 0.1(arbitrary units) for GaAs, mono- and polycrystalline ZnSe antenna, respectively. We can conclude that the THz field amplitudes saturate to the same absolute value, which is expected in the THz-field-screening saturation regime.

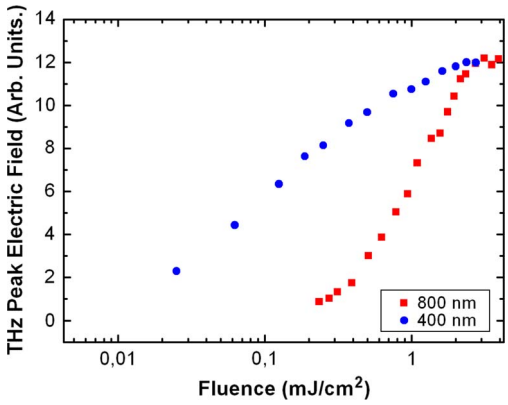

Fig. 5. Fluence dependence of the peak THz electric field from ZnSe single crystal antenna illuminated at 400 nm and 800 nm.

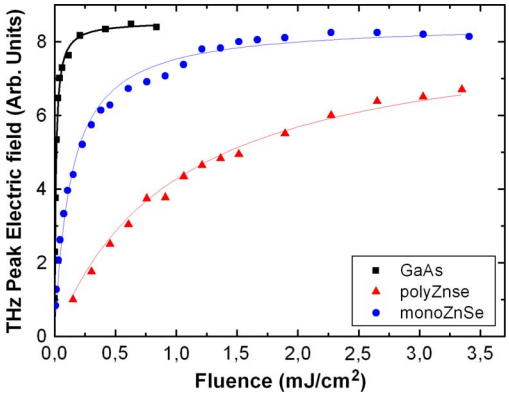

Fig. 6. Fluence dependence of peak field of THz radiation from GaAs, ZnSe single crystal, and polycrystalline ZnSe photoconductive antenna. Squares are the experimental data, and solid lines are fits to the data based on (5).

Fig. 7 shows the THz peak electric field from ZnSe single crystal and GaAs antennas as a function of the bias voltage. Both antennas have been pumped above the bandgap (800 nm for the GaAs antenna and 400 nm for the ZnSe single crystal antenna). The fluence was fixed at 92 μJ cm^{-2} for the GaAs antenna and 700 μJ cm^{-2} for the ZnSe single crystal antenna. These two fluences were chosen to be over the saturation fluence for each crystal. Breakdown of the GaAs antenna was observed at 11 kV/cm, but for the ZnSe single crystal antenna, breakdown was not observed even at bias fields of 14 kV/cm. Fig. 7 shows that compared with GaAs, stronger THz electric fields are radiated with the ZnSe single crystal antenna. Also, Fig. 7 shows that the two curves have different slopes. The slope of the GaAs antenna is higher than the slope of the ZnSe single crystal antenna because of the different saturation fluences. This results in a slightly higher THz peak field with a GaAs antenna at 92 μJ cm^{-2}, compared with a ZnSe single crystal antennas at 700 μJ cm^{-2} (cf. Fig. 6), which in turn results in a higher slope for the GaAs antenna seen in Fig. 7.

4. Discussion

In the previous section, the fluence dependence and the bias voltage dependence of mono- and polycrystalline ZnSe antennas was presented. The comparison of the THz radiation between ZnSe antennas and GaAs antennas was also presented. These results allow us to calculate, compare,

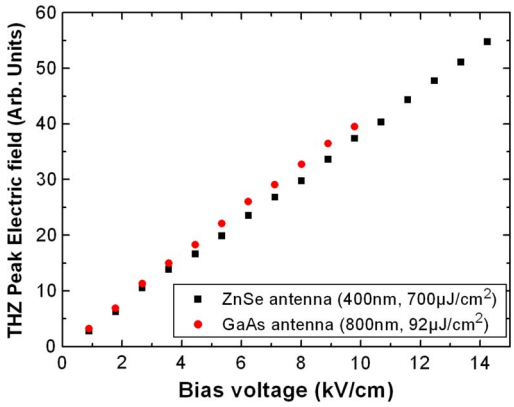

Fig. 7. Comparison of bias field dependence of the peak THz electric field for GaAs antenna excited at 800 nm and single crystal ZnSe antenna excited at 400 nm.

TABLE 1

Parameters Used in the Calculation of the Optical to THz Conversion Efficiency Based on (4) as Presented in Fig. 8

Parameters	*GaAs*	*ZnSe single crystal*
Carrier mobility μ (cm^2/vs)	**4000**	**267**
Saturation fluence F_{sat} (μJcm^{-2})	**10.5**	**150**
1/e THz pulse length duration τ (ps)	**0,9**	**0,56**

and discuss the optical-to-THz energy conversion efficiency and to examine which emitter is more efficient and under what conditions it should be operated.

Since THz emission from photoconductive switches extracts energy from the bias field, photoconductive antennas are expected to have a high optical-to-THz energy conversion efficiency, making it attractive as a high-energy THz source. It was demonstrated that with the same antenna design, higher THz electric fields could be generated with ZnSe photoconductive switches and, therefore higher THz pulse energy in comparison with GaAs antennas. In this section, the scaling behaviors investigated in previous sections will be used to demonstrate that we can expect to have a better optical-to-THz energy conversion efficiency with ZnSe antennas than GaAs antennas.

First, we examine the question of which emitter most efficiently converts optical energy to THz energy. In the experiments, breakdown fields occur at 11 kV/cm in GaAs antennas. Nonetheless, it is safer not to apply bias fields higher than 10 kV/cm so that the GaAs crystal is not damaged. On the other hand, for ZnSe antennas, breakdown did not occur with bias fields of 23 kV/cm. However, it has been reported that ZnSe switches can withstand applied bias fields of up to 80 kV/cm [32]. Also, Holzman *et al.* worked with up to 125 kV/cm bias voltage with polycrystalline ZnSe photoconductive antennas, pumped below bandgap, and did not observe saturation of the THz electric field [27]. From (4), we calculate the maximum THz conversion efficiency expected from a GaAs and ZnSe single crystal photoconductive antenna at different bias fields. The values used in the calculation are summarized in Table 1. The results are plotted in Fig. 8.

Fig. 8 shows the quadratic dependence of the maximum efficiency on the applied bias field. As we can see in Fig. 8, the maximum optical-to-THz conversion efficiency is lower with a ZnSe photoconductive antenna at a bias field of 23 kV/cm, compared with a GaAs antenna at bias field of 10 kV/cm (7.13×10^{-4} versus 2.84×10^{-3}).

However, it is not possible to apply bias fields higher than 11 kV/cm on a GaAs antenna without breakdown. If we apply a bias field of 48 kV/cm to a ZnSe single crystal antenna, we could expect an optical-to-THz energy conversion efficiency equal to that of a GaAs antenna with a bias field of 10 kV/cm. To apply such bias field, the antenna must be placed in a vacuum because the

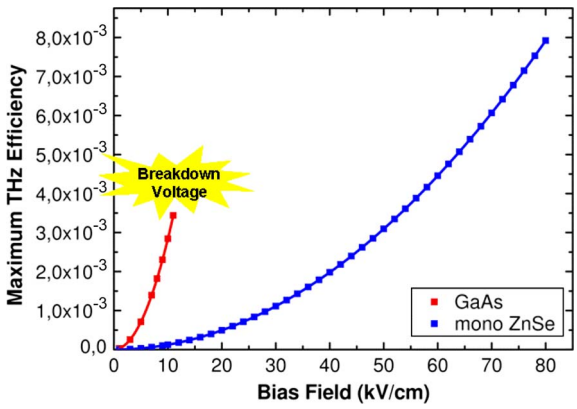

Fig. 8. Maximum THz efficiency versus applied bias field for ZnSe single crystal antennas and GaAs antennas excited above the bandgap.

breakdown voltage of air at atmospheric pressure and room temperature is around 30 kV/cm. However, if we are able to apply a bias field of 80 kV/cm with ZnSe antennas, we could expect to have a maximum optical-to-THz efficiency of 7.92×10^{-3}, which is approximately three times higher than the efficiency with GaAs antennas. Operating with the ZnSe is more complicated, however, because it requires pumping above the 2.67 eV bandgap, which requires a frequency doubling crystal, such as BBO, to generate the second harmonic of the Ti:sapphire laser, which has an efficiency that is usually in the range of 30–40%. Under these conditions, we can expect that the optical-to-THz energy conversion efficiency from ZnSe antennas, including the conversion of the frequency doubling crystal, is competitive with the 800-nm optical-to-THz energy conversion efficiency of GaAs antennas.

The optical-to-THz energy conversion efficiency values calculated in Table 1 are the expected values based on (4). The THz electric field was not calibrated in these experiments because of the difficulty in measuring the THz beam spot profile and calibrating the linear electrooptic response of the ZnTe crystal. Nonetheless, in Table 1, we calculate a maximum optical-to-THz efficiency with GaAs antennas at 10 kV/cm of 2.84×10^{-3}, which is slightly higher than the 1.6×10^{-3} efficiency that You *et al.* obtained when they generated 0.8 μJ THz pulses [19]. The difference could be attributed to the 40 μJ/cm^2 fluence that You *et al.* used to excite the GaAs antenna, which corresponds to a fluence around four times higher than the saturation fluence. Equation (4) is also an approximate expression that can be expected to be reasonable to within a factor of two. It does not take into account the THz pulse characteristics in space for example.

Next, to ensure that the estimates made above are realistic, we calculate and compare the ratio δ between the optical-to-THz energy conversion efficiency of ZnSe antennas and the optical-to-THz energy conversion efficiency of GaAs antennas. δ can be expressed as

$$W_{\mathrm{THz}} \approx \frac{A\left|E_{\mathrm{THz}}^{pk}\right|^2}{2_0}. \tag{6}$$

Here, η is the optical-to-THz conversion efficiency, which is defined by

$$\eta = \left(\frac{W_{\mathrm{THz}}}{W_{inp}}\right). \tag{7}$$

Here, W_{inp} is the optical energy and W_{THz} is the THz energy, which can be approximated by [23]

$$W_{\mathrm{THz}} \approx \frac{\tau A\left|E_{\mathrm{THz}}^{pk}\right|^2}{2\eta_0}. \tag{8}$$

TABLE 2

Parameters Used in the Estimation Using (13) of the Ratio of Optical to THz Conversion Efficiency Between a ZnSe Antenna and a GaAs Antenna

Parameters	*GaAs*	*ZnSe single crystal*
THz peak electric field (Arb. Units)	**4.26**	**4.26**
Bias field (kV/cm)	**3**	**3**
Optical energy W_{in} (μJ/cm^2)	**10.5 (800 nm)**	**133 (400 nm)**
1/e pulse length duration τ (ps)	**2.39**	**2**
Ratio of efficiency δ	**6.6×10^{-2}**	

Here, τ is the 1/e THz pulse width, A is the area of the THz beam at the detector, and E_{THz} is the THz peak electric field. When the THz peak electric field from ZnSe antenna is equal to the THz peak electric field of the GaAs antenna, and if we assume that the area of the THz beam on the crystal detector for ZnSe and GaAs antenna are equal, δ becomes

$$\delta \approx \left(\frac{\tau_{ZnSe} W_{in,GaAs}}{\tau_{GaAs} W_{in,ZnSE}}\right). \tag{9}$$

Table 2 summarizes the different parameters of GaAs and ZnSe single crystal antennas during the experiments of Fig. 5, where we compared the THz radiation from ZnSe and GaAs antennas.

From Table 2, we find that the ratio $\delta = 6.6 \times 10^{-2}$ between the optical-to-THz efficiency for the ZnSe single crystal antenna and the GaAs antenna at a bias field of 3 kV/cm and with fluence close to the saturation fluence. In comparison, the same ratio δ from the optical-to-THz efficiency calculated from Table 1 at 3 kV/cm for ZnSe and GaAs antenna is 4.3×10^{-2}. The two results are comparable. Therefore, the results in Table 2 indicate that our calculated optical-to-THz energy conversion efficiency with ZnSe antennas in Table 1 is realistic.

Based on our experiments and on (4), we showed in this section that ZnSe single crystal antennas excited above the bandgap could operate with higher optical-to-THz energy conversion efficiency, in comparison with GaAs antennas or optical rectification sources (i.e., ZnTe and $LiNbO_3$ sources). Thus, there is strong incentive to work with ZnSe antennas pumped above the bandgap to create an intense THz source with high THz pulse energy using an amplified Ti:sapphire laser and a moderate-sized crystal. For example, if we work with a 6-cm gap ZnSe single crystal antenna, we will require a pump laser of at least 5.5 mJ at 400 nm (around 16 mJ at 800 nm) to work at the saturation fluence. With a THz efficiency of 7.92×10^{-3}, we expect to generate THz pulse energy of 43 μJ. On the other hand, if we were to work with GaAs antennas and generate THz pulse energy of 43 μJ, we would require at least 15 mJ (2.84×10^{-3} THz efficiency) to work at the saturation fluence (10.5 μJ/cm^2) at 800 nm, which requires a 38-cm gap size GaAs antenna. Working with such a large antenna and laser beam size is highly inconvenient, requiring one to work with large optics and crystals. With this very simple example, we can see that in comparison with a GaAs antenna, scaling up to high THz energy using ZnSe single crystal antennas is advantageous because of its higher optical-to-THz energy conversion efficiency and its higher saturation fluence. We should note that the use of high bias fields (80 kV/cm) to the ZnSe antennas requires one to work in a vacuum. At the ALLS laboratory of the INRS, we have already developed a THz source with large ZnTe crystal that is placed in a vacuum, which can generate a 1.5-μJ THz pulse [6]. Once the scaling up of the ZnSe single crystal antenna is completed, we plan to pump the ZnSe antenna with the 100-Hz laser at the ALLS laboratory using this vacuum chamber.

5. Conclusion

In conclusion, we have generated THz radiation with ZnSe large aperture photoconductive antennas excited above and below the bandgap. We demonstrated that it is unfavorable to work below the bandgap, because of the low optical-to-THz conversion efficiency and thermal runaway

of the antenna. We also demonstrated that it is more advantageous to work with ZnSe single crystal than with CVD polycrystalline ZnSe, due to the higher mobility in the single crystal ZnSe, which results in higher optical-to-THz conversion efficiency. Finally, we compared the performance of ZnSe and GaAs antennas, and we conclude that higher THz electric fields can be generated with ZnSe antennas and higher THz pulse energies and that ZnSe antennas are expected to have a higher optical-to-THz conversion efficiency compared with GaAs antennas. While the higher conversion efficiency in ZnSe requires a more complicated set-up than GaAs, the advantages over GaAs become clear when scaling to high optical energies, which are particularly interesting for investigating nonlinear THz-matter interactions.

Acknowledgment

The authors are thankful to R. Helsten for his technical assistance with the Ultrafast Optical Processing Ti:sapphire laser source. The authors are also grateful for support from the Natural Sciences and Engineering Research Council of Canada.

References

[1] B. Ferguson and X.-C. Zhang, "Materials for terahertz science and technology," *Nat. Mater.*, vol. 1, no. 1, pp. 26–33, Sep. 2002.
[2] K. Humphreys, J. P. Loughran, M. Gradziel, W. Lanigan, T. Ward, J. A. Murphy, and C. O'Sullivan, "Medical applications of terahertz imaging: A review of current technology and potential applications in biomedical engineering," in *Proc. 26th Annu. Int. Conf. IEEE EMBS*, 2004, pp. 1302–1305.
[3] W. L. Chan, J. Deibel, and D. M. Mittleman, "Imaging with terahertz radiation," *Rep. Prog. Phys.*, vol. 70, no. 8, pp. 1325–1379, Aug. 2007.
[4] J. F. Federici, B. Schulkin, F. Huang, D. Gary, R. Barat, F. Oliveira, and D. Zimdars, "THz imaging and sensing for security applications—Explosives, weapons and drugs," *Semicond. Sci. Technol.*, vol. 20, no. 7, pp. S266–S280, Jul. 2005.
[5] C. A. Schmuttenmaer, "Exploring dynamics in the far-infrared with terahertz spectroscopy," *Chem. Rev.*, vol. 104, no. 4, pp. 1759–1779, Apr. 2004.
[6] F. Blanchard, L. Razzari, H. C. Bandulet, G. Sharma, R. Morandotti, J. C. Kieffer, T. Ozaki, M. Reid, H. F. Tiedje, H. K. Haugen, and F. A. Hegman, "Generation of 1.5 μJ single-cycle terahertz pulses by optical rectification from a large aperture ZnTe crystal," *Opt. Express*, vol. 15, no. 20, pp. 13 212–13 220, Oct. 2007.
[7] J. Hebling, G. Almasi, I. Z. Kozma, and J. Kuhl, "Velocity matching by pulse front tilting for large area THz-pulse generation," *Opt. Express*, vol. 10, no. 21, pp. 1161–1166, Oct. 2002.
[8] K.-L. Yeh, M. C. Hoffmann, J. Hebling, and K. A. Nelson, "Generation of 10 μJ ultrashort terahertz pulses by optical rectification," *Appl. Phys. Lett.*, vol. 90, no. 17, p. 171 121, Apr. 2007.
[9] J. Hebling, K.-L. Yeh, M. C. Hoffmann, B. Bartal, and K. A. Nelson, "Generation of high-power terahertz pulses by tilted-pulse-front excitation and their application possibilities," *J. Opt. Soc. Amer. B, Opt. Phys.*, vol. 25, no. 7, pp. B6–B19, Jul. 2008.
[10] J. A. Fulop, L. Palfalvi, G. Almasi, and J. Hebling, "Design of high energy THz sources based on optical rectification," *Opt. Express*, vol. 18, no. 12, pp. 12 311–12 327, Jun. 2010.
[11] A. G. Stepanov, L. Bonacina, S. V. Chekalin, and J.-P. Wolf, "Generation of 30 μJ single-cycle terahertz pulses at 100 Hz repetition rate by optical rectification," *Opt. Lett.*, vol. 33, no. 21, pp. 2497–2499, Nov. 2008.
[12] O. E. Martinez, "Pulse distortions in tilted pulse schemes for ultrashort pulses," *Opt. Commun.*, vol. 59, no. 3, pp. 229–232, Sep. 1986.
[13] L. Razzari, F. H. Su, G. Sharma, F. Blanchard, A. Ayesheshim, H.-C. Bandulet, R. Morandotti, J. C. Kieffer, T. Ozaki, M. Reid, and F. A. Hegmann, "Nonlinear ultrafast modulation of the optical absorption of intense few-cycle terahertz pulses in n-doped semiconductors," *Phys. Rev. B, Condens. Matter*, vol. 79, no. 19, p. 193 204, May 2009.
[14] F. H. Su, F. Blanchard, G. Sharma, L. Razzari, A. Ayesheshim, T. L. Cocker, L. V. Titova, T. Ozaki, J. C. Kieffer, R. Morandotti, M. Reid, and F. A. Hegmann, "Terahertz pulse induced intervalley scattering in photoexcited GaAs," *Opt. Express*, vol. 17, no. 12, pp. 9620–9629, Jun. 2009.
[15] G. Sharma, L. Razzari, F. H. Su, F. Blanchard, A. Ayesheshim, T. L. Cocker, L. V. Titova, H. C. Bandulet, T. Ozaki, J.-C. Kieffer, R. Morandotti, M. Reid, and F. A. Hegmann, "Time-resolved terahertz spectroscopy of free carrier nonlinear dynamics in semiconductors," *IEEE Photon. J.*, vol. 2, no. 4, pp. 578–592, Aug. 2010.
[16] M. C. Hoffmann, J. Hebling, H. Y. Hwang, K.-L. Yeh, and K. A. Nelson, "THz-pump/THz-probe spectroscopy of semiconductors at high field strengths [Invited]," *J. Opt. Soc. Amer. B, Opt. Phys.*, vol. 26, no. 9, pp. A29–A34, Sep. 2009.
[17] M. C. Hoffmann, N. C. Brandt, H. Y. Hwang, K.-L. Yeh, and K. A. Nelson, "Terahertz Kerr effect," *Appl. Phys. Lett.*, vol. 95, no. 23, p. 231 105, Dec. 2009.
[18] D. You, R. Jones, and P. Bucksbaum, "Generation of high power sub-single cycle 500 fs electromagnetic pulses," *Opt. Lett.*, vol. 18, no. 4, pp. 290–292, Feb. 1993.
[19] J. T. Darrow, X. C. Zhang, D. H. Auston, and J. D. Morse, "Saturation properties of large-aperture photoconducting antennas," *IEEE J. Quantum Electron.*, vol. 28, no. 6, pp. 1607–1616, Jun. 1992.

[20] M. R. Stone, M. Naftaly, R. E. Miles, J. R. Fletcher, and D. P. Steenson, "Electrical and radiation characteristics of semilarge photoconductive emitters," *IEEE Trans. Microw. Theory Tech.*, vol. 52, no. 10, pp. 2420–2429, Oct. 2004.
[21] T. Hattori, K. Egawa, S. Ookuma, and T. Itatani, "Intense THz pulses from large-aperture with interdigitated electrodes," *Jpn. J. Appl. Phys.*, vol. 45, pp. L422–L424, 2006.
[22] P. K. Benicewicz, J. P. Roberts, and A. J. Taylor, "Scaling of terahertz radiation from large-aperture biased photoconductors," *J. Opt. Soc. Amer. B, Opt. Phys.*, vol. 11, no. 12, pp. 2533–2546, Dec. 1994.
[23] M. Reid and R. Fedosejevs, "Quantitative comparison of terahertz emission from (100) InAs surfaces and a GaAs large-aperture photoconductive switch at high fluences," *Appl. Opt.*, vol. 44, no. 1, pp. 149–153, Jan. 2005.
[24] H. Yoneda, K. Tokuyama, K. Ueda, H. Yamamoto, and K. Baba, "High power terahertz radiation emitter with a diamond photoconductive switch array," *Appl. Opt.*, vol. 40, no. 36, pp. 6733–6736, Dec. 2001.
[25] P. S. Cho, P.-T. Ho, J. Goldhar, and C. H. Lee, "Photoconductivity in ZnSe under high electric fields," *IEEE J. Quantum Electron.*, vol. 30, no. 6, pp. 1489–1497, Jun. 1994.
[26] I. Kikuma, M. Matsuo, and T. Komuro, "In situ annealing of melt-Grown ZnSe crystals under Zn partial pressure," *Jpn. J. Appl. Phys.*, vol. 31, no. 5A, pp. L531–L534, May 1992.
[27] J. F. Holzman and A. Y. Elezzabi, "Two-photon photoconductive terahertz generation in ZnSe," *Appl. Phys. Lett.*, vol. 83, no. 14, pp. 2967–2969, Oct. 2003.
[28] A. Y. Elezzabi, H. Houtman, and J. Meyer, "Time-resolved impact ionization in ZnSe high-voltage switches," *IEEE Trans. Plasma Sci.*, vol. 22, no. 6, pp. 1043–1048, Dec. 1994.
[29] Q. Wu, M. Litz, and X.-C. Zhang, "Broadband detection capability of ZnTe electro-optic field detector," *Appl. Phys. Lett.*, vol. 68, no. 21, pp. 2924–2926, May 1996.
[30] R. A. Cheville and D. A. Grischkowsky, "Far-infrared foreign and self-broadened rotational linewidths of high-temperature water vapor," *J. Opt. Soc. Amer. B, Opt. Phys.*, vol. 16, no. 2, pp. 317–322, Feb. 1999.
[31] T. Hattori, K. Tukamoto, and H. Nakatsuka, "Time-resolved study of intense THz pulses generated by a large-aperture photoconductive antenna," *Jpn. J. Appl. Phys.*, vol. 40, no. 8, pp. 4907–4912, Aug. 2001.
[32] T. Löffler, F. Jacob, and H. G. Roskos, "Generation of THz pulses by photoionisation of electrically biased air," *Appl. Phys. Lett.*, vol. 77, no. 3, pp. 453–455, Jul. 2000.